STABILITY AND EFFECTIVENESS OF A DSA SCHEME HAVING TWO DIFFUSION CELLS PER TRANSPORT CELL

A Thesis

by

JOHNATHAN R. GRISSOM

Submitted to the Graduate and Professional School of
Texas A&M University
in partial fulfillment of the requirements for the degree of

MASTER OF SCIENCE

Chair of Committee,	Jim Morel
Committee Members,	Marvin Adams
	Jean Ragusa
	Matthias Maier
Head of Department,	Michael Nastasi

May 2022

Major Subject: Nuclear Engineering

ABSTRACT

The purpose of this thesis is to detail the analysis on the stability and effectiveness of a DSA scheme having two diffusion cells per transport cell. The inspiration to look into such a scheme originated from Ryosuke Park's recently published work on an unconditionally stable HOLO scheme, however, it should be noted that what we analyzed is not equivalent to Ryosuke's method. The only concept from his method explored in this thesis was the idea of having two diffusion cells per transport cell. To accomplish this, a homogeneous, 1-D slab geometry version of the S_N equations with isotropic scattering, and a zero distributed source was discretized with a standard lumped linear-discontinuous Galerkin source iteration scheme and accelerated with a cell-centered diffusion equation for the iterative errors in the scalar fluxes on a sub-mesh for the preconditioning step. A test problem with an incident flux and reflective boundary conditions on a 1000 cm slab was used to experimentally measure the spectral radius. A Fourier analysis was also performed on the error reduction matrix of the full scheme to analytically measure the spectral radius under the same conditions as the experiment. Both of these results were in agreeance and showed that having two diffusion cells per transport cell by itself does not lead to an unconditionally stable system.

DEDICATION

To my mother and father, who have sacrificed much throughout their lives so that their children could have the opportunities they never had. Were it not for them, my pursuit of higher education would have never been possible. Thank you.

CONTRIBUTORS AND FUNDING SOURCES

Contributors

This work was supported by a thesis committee consisting of Professors Jim Morel [advisor], Marvin Adams, and Jean Ragusa of the Department of Nuclear Engineering and Professor Matthias Maier of the Department of Mathematics. Inspiration of the method analyzed came from the work of Ryosuke Park at Los Alamos National Laboratory, however this is not an analysis of his method. All other work conducted for the thesis was completed by the student independently.

Funding Sources

Graduate study was supported by Texas A&M University for work done as a teaching assistant.

NOMENCLATURE

HOLO	High-Order Low-Order
DSA	Diffusion Synthetic Acceleration
NDA	Non-Linear Diffusion Acceleration
LDG	Lumped Linear Discontinuous Galerkin
N	Particle Number
ϕ	Scalar Flux
ψ	Angular Flux
σ_t	Total Interaction Macroscopic Cross-Section
σ_s	Scattering Macroscopic Cross-Section
D	Diffusion Coefficient
Q	Distributed Source

TABLE OF CONTENTS

Page

LIST OF TABLES

TABLE Page

1. INTRODUCTION

1.1 Background

Within the nuclear industry there exists a growing need for efficient and accurate modeling of complex systems to justify designs, experiments, and even national policy. These systems can vary across a wide range of applications from fission reactor designs, inertial confinement fusion, astrophysics, health physics, and non-proliferation. In each of these cases, many different physical phenomena must be accurately represented. In particular, accurate representation of the radiation transport within these systems is of the utmost importance. The accurate representation of radiation transport by itself can be complex, and is often further complicated in problems of interest due to coupling with other complex physical phenomena, such as in problems involving radiation hydrodynamics. This can result in models that require excessive computational runtime, incurring extra costs to investors. Thus, not only do these models have to be accurate, they must also be computationally efficient. It is with this goal in mind, that research into various numerical methods in radiation transport is often inspired, and is certainly an inspiration for this thesis.

1.1.1 Radiation Transport

In order to accurately represent the effects of radiation within a system, physical conservation laws are applied to the distribution of particles within the entire phase space of the system (position, angular direction, and energy). This is typically done by setting the rate of change of particle number within the phase space equal to the difference between the source rate within the phase space and the loss rate within the phase space. The resulting equation is the Boltzmann transport equation, initially devised by Ludwig Boltzmann to describe thermodynamic properties of gases, but can be applied to particles as well:

$$\frac{d}{dt}(N) = (Sources) - (Sinks), \tag{1.1}$$

which, for neutron transport becomes:

$$\frac{1}{v}\frac{\partial\psi}{\partial t} = Q + \int_0^\infty \int_{4\pi} \sigma_s(E' \to E, \vec{\Omega}' \cdot \vec{\Omega})\psi(E', \vec{\Omega})d\vec{\Omega}'dE' - \vec{\Omega} \cdot \vec{\nabla}\psi - \sigma_t\psi, \tag{1.2}$$

where:

$$\psi(\vec{r}, \vec{\Omega}, E, t)dP \equiv \text{Angular Neutron flux}, \tag{1.3}$$

$$\frac{1}{v}\frac{\partial\psi}{\partial t}dP \equiv \text{Rate of change of neutron number}, \tag{1.4}$$

$$QdP \equiv \text{Rate of neutrons born into the phase space}, \tag{1.5}$$

$$\int_0^\infty \int_{4\pi} \sigma_s(E' \to E, \vec{\Omega}' \cdot \vec{\Omega})\psi(E', \vec{\Omega})d\vec{\Omega}'dE'dP \equiv \text{Rate of neutrons scattered}, \tag{1.6}$$

$$\vec{\Omega} \cdot \vec{\nabla}\psi dP \equiv \text{Rate of net advection}, \tag{1.7}$$

$$\sigma_t\psi dP \equiv \text{Rate of removal due to interactions}. \tag{1.8}$$

The Boltzmann transport equation describes the physical phenomena that affects particle transport throughout a system, and can be used to describe the resulting particle density. When particles interact with the medium, changes to other material properties, such as pressure, temperature, and material density, can occur. These non-linearities can introduce difficulties, but many of the numerical approaches remain the same.

1.1.2 Relevant Numerical Methods

Numerical methods used to solve the Boltzmann transport equation fall into two primary categories: stochastic methods, such as Monte Carlo, and deterministic methods, such as the discrete-ordinates S_N approximation.[1] For our study, it is sufficient to just review the S_N method as applied to the steady-state, mono-energetic Boltzmann equation with isotropic scattering:

$$\vec{\Omega} \cdot \vec{\nabla}\psi + \sigma_t\psi = \frac{\sigma_s}{2}\phi + \frac{Q}{2}, \tag{1.9}$$

where:

$$\phi = \int_{4\pi} \psi(\vec{\Omega}) d\vec{\Omega} \equiv \text{Scalar Flux.} \tag{1.10}$$

The steady-state, mono-energetic Boltzmann equation is discretized across the spatial domain of interest using one of many possible schemes, as well as over angle using collocation at Gauss quadrature points. The scalar flux is computed using the quadrature formula:

$$\phi = \int_{-1}^{+1} \psi(\mu) d\mu \approx \sum_{n=1}^{N} \psi_n w_n. \tag{1.11}$$

This is then solved iteratively until it converges to a solution within some tolerance. If we re-express equation (1.9) into a reduced version with L representing the sinks ($\vec{\Omega} \cdot \vec{\nabla}\psi + \sigma_t \psi$), S representing the scattering source ($\frac{\sigma_s}{2}$), and l representing the iteration index, then the source iteration approach can be described as follows:

$$L\psi^{l+1} = S\phi^l + \frac{Q}{2}\ ,\ l \geq 0. \tag{1.12}$$

Starting with an initial guess for ψ and appropriate boundary conditions, the system of linear equations can be solved for the next iterate by inverting L. This can be repeated until a set number of iterations have been completed or until some convergence criteria is met. Given a zero initial guess, ψ^l represents the flux due to (l) scatters, thus it is easy to see that problems with weak scattering converge very quickly while scattering dominated problems will converge slowly. Increasing the efficiency of source iteration in these high scattering problems is of great practical importance.

Over the years many strategies have been developed to improve S_N iterative methods. This has resulted in methods such as Non-Linear Diffusion Acceleration (NDA) and its linear equivalent, Diffusion Synthetic Acceleration (DSA), where a preconditioning diffusion step is taken during each iteration to improve the next iterate guess.[2][3][4][5][6][7] Depending on the problem, this can reduce the number of iterations required for convergence by orders of magnitude. Other meth-

ods such as quasi-diffusion and High-Order Low-Order (HOLO) methods have also been developed in a similar sense, however unlike true acceleration methods, the high order and low order methods do not necessarily converge to the same solution.[8][9] In both of these approaches, it is important to ensure that the combined methods are unconditionally stable for the high-scattering problems of interest. In particular, inconsistent differencing of the accelerated iteration equations can lead to conditionally unstable schemes.[4]

1.2 Motivation for Work

Recently, Ryosuke Park from Los Alamos National Laboratory published a paper on an asymptotic thick diffusion limit preserving HOLO method for use in thermal radiation transport. In this paper he couples high order S_N equations spatially discretized with a lumped linear discontinuous Galerkin (LDG) approximation to a low order cell-centered diffusion equation on a sub-mesh with two diffusion cells per transport cell.[7][10] The manner in which he does this is very similar, though not equivalent, to NDA. The results of his work indicate that this method is unconditionally stable. This has sparked curiosity due to its similarities to NDA and the fact that it is documented that a lack of consistent differencing between the high order and low order equations often results in conditionally unstable NDA schemes. However, Park's method is not a true acceleration scheme since the high order and low order scalar fluxes are not necessarily the same upon iterative convergence of his HOLO method. Thus, it is not clear if the stability of his scheme arises from the particular way that the correction terms are defined or the fact that there are two diffusion cells per S_N cell. To shed light on this question, we have defined a DSA scheme somewhat analogous to Park's HOLO scheme in order to analyze the effects of having two diffusion cells per S_N cell. In particular, the S_N equations will be spatially discretized using the standard lumped linear-discontinuous scheme, and the diffusion discretization will be the standard cell-centered scheme, but with two diffusion cells per S_N cell. There will be no need for correction terms as the diffusion equation will be used to compute the iterative error in the scalar flux rather than the accelerated flux itself. It is the purpose of this research to investigate the stability and effectiveness of this particular DSA scheme with two diffusion cells per S_N cell.

1.3 Thesis Organization

The organization of the rest of this thesis is as follows: In Section 2 we describe the method being analyzed in full detail, starting with the general 1-D, steady-state, mono-energetic S_N equations on a slab. Next we derive the proposed DSA scheme with two diffusion cells per S_N cell. This is accompanied with a description of our computational script to compute the spectral radius of this method under various scattering to total cross-section ratios and cell widths. In Section 3 we describe the Fourier analysis performed on the method along with its detailed derivation. In Section 4, the results of both the numerical experiment and the Fourier analysis are presented and discussed. This is preceded by a full description of the various test cases we have tested. And finally, in Section 5, the thesis concludes with a summarization of our work, results, and possible directions for related future work.

2. DERIVATION OF NUMERICAL SCHEME

2.1 Transport Problem of Interest

The transport problem we apply our proposed DSA scheme to is a homogeneous, 1-D slab geometry version of the problem detailed in equation (1.9) with isotropic scattering and an isotropic distributed source. The scheme is a two-step iteration scheme, where the transport step solves the discrete ordinates S_N equations spatially discretized using a lumped linear-discontinuous Galerkin scheme and the diffusion correction step is spatially discretized using the standard cell-centered scheme on a sub-mesh. In the diffusion step, we directly solve for the iterative error on the interpolated flux, extrapolate out to the transport unknown locations, and then apply the error as a correction for the $l+1$ iterate as follows:

$$-\frac{\partial}{\partial x}D\frac{\partial \xi}{\partial x}+\sigma_a\xi=\sigma_s(\phi^{l+\frac{1}{2}}-\phi^{l}), \tag{2.1}$$

where:

$$\xi=\phi^{exact}-\phi^{l+\frac{1}{2}}\equiv\text{Iterate Error}, \tag{2.2}$$

$$\phi^{l+1}=\xi+\phi^{l+\frac{1}{2}}, \tag{2.3}$$

$$D=\frac{1}{3\sigma_t}\equiv\text{Diffusion Coefficient}. \tag{2.4}$$

The iteration is continued until some tolerance parameter is met and the solution has converged. Our tests use the zero source version of this problem, allowing for the iterative solution to be the error, avoiding roundoff difficulties or scenarios where the solution coverges before the spectral radius. The boundary conditions used in the problem of interest are a reflective condition on the interior (left) boundary and a vacuum on the exterior (right) boundary.

2.2 Numerical Scheme

The following section details the derivation of this acceleration scheme. Starting with equation (1.9), the assumptions of isotropic scattering, isotropic distributed source, and a homogenous, 1-D slab geometry are made. This is followed by performing the standard discrete ordinates S_N angular discretization. Then, the system is spatially discretized using the standard lumped linear-discontinuous Galerkin scheme. This defines the the source iteration equation first used in a two-step iteration. Finally, the cell-centered diffusion equation for the iterative errors in the scalar fluxes from the source iteration step is derived on a sub-mesh.

2.2.1 Angular Discretization with the Discrete Ordinates Method

Starting with the steady-state, mono-energetic Boltzmann equation described in equation (1.9), we rewrite our angular terms in terms of their discrete angular cosines over the domain $[-1, +1]$:

$$\mu \frac{d\psi}{dx} + \sigma_t \psi = \frac{\sigma_s}{2}\phi + \frac{Q}{2} \tag{2.5}$$

where:

$$\mu = cos(\theta). \tag{2.6}$$

We then apply the definition of scaler flux and collocate using a Gauss-Legendre quadrature, where the quadrature points, denoted by n, are chosen so that they are the same as the discrete angles, denoted by m. The result is a scheme that can be iterated to solve for the scalar flux by lagging the scattering source term:

$$\mu_m \frac{d\psi_m^{l+\frac{1}{2}}}{dx} + \sigma_t \psi_m^{l+\frac{1}{2}} = \frac{\sigma_s}{2}\phi^l + \frac{Q}{2} \tag{2.7}$$

$$\phi = \int_{-1}^{+1} \psi_m(\mu) d\mu \approx \sum_{n=1}^{N} \psi_n w_n. \tag{2.8}$$

For DSA, we still lag the scattering source, but the resulting angular fluxes are used to calculate the half-step scalar flux that is used in the diffusion acceleration step. For simplicity, the indexing

for the discrete angles and quadrature points are dropped in later equations in this thesis.

2.2.2 Spatial Discretization with the Lumped Linear-Discontinuous Galerkin Scheme

The resulting equation (2.7) is discretized using a lumped linear-discontinuous Galerkin scheme, yielding a set of equations for both the positive angular cosines and the negative angular cosines. Homogeneous material properties are assumed across the 1-D slab so that the only property varying on each cell is the neutron flux. The cell width is set to h for all cells on the domain.

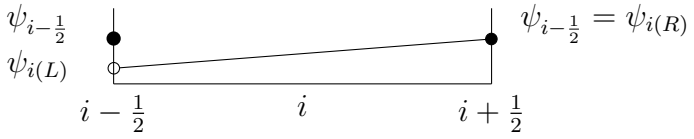

This results in the following system of equations:

$$\mu > 0 : \mu[\psi_i - \psi_{i-\frac{1}{2}}] + \frac{\sigma_t h}{2}\psi_{i(L)} = \frac{\sigma_s h}{4}\phi_{i(L)} + \frac{h}{4}Q, \tag{2.9}$$

$$\mu > 0 : \mu[\psi_{i+\frac{1}{2}} - \psi_i] + \frac{\sigma_t h}{2}\psi_{i(R)} = \frac{\sigma_s h}{4}\phi_{i(R)} + \frac{h}{4}Q, \tag{2.10}$$

$$\mu < 0 : \mu[\psi_i - \psi_{i-\frac{1}{2}}] + \frac{\sigma_t h}{2}\psi_{i(L)} = \frac{\sigma_s h}{4}\phi_{i(L)} + \frac{h}{4}Q, \tag{2.11}$$

$$\mu < 0 : \mu[\psi_{i+\frac{1}{2}} - \psi_i] + \frac{\sigma_t h}{2}\psi_{i(R)} = \frac{\sigma_s h}{4}\phi_{i(R)} + \frac{h}{4}Q. \tag{2.12}$$

The interior flux, ψ_i, within each spatial cell is defined in terms of the edge fluxes by averaging them across the cell:

$$\psi_i = \frac{1}{2}[\psi_{i(L)} + \psi_{i(R)}]. \tag{2.13}$$

The scattering source term in these equations is lagged by using the previous iteration's edge fluxes, as done in equation (2.7). By up-winding the flux, and applying the proper boundary conditions for the exterior cells, the system becomes solvable on each interior cell:

$$\mu > 0 : \psi_{i-\frac{1}{2}} = \psi_{i-1(R)}, \quad \psi_{i+\frac{1}{2}} = \psi_{i(R)}, \tag{2.14}$$

$$\begin{bmatrix} \frac{\mu}{2} + \frac{\sigma_t h}{2} & \frac{\mu}{2} \\ -\frac{\mu}{2} & \frac{\mu}{2} + \frac{\sigma_t h}{2} \end{bmatrix} \begin{bmatrix} \psi_L \\ \psi_R \end{bmatrix} = \begin{bmatrix} \frac{\sigma_s h}{4}\phi_L + \frac{hQ}{4} + \mu\psi_{i-\frac{1}{2}} \\ \frac{\sigma_s h}{4}\phi_R + \frac{hQ}{4} \end{bmatrix}, \tag{2.15}$$

$$\mu < 0 : \psi_{i+\frac{1}{2}} = \psi_{i+1(L)}, \quad \psi_{i-\frac{1}{2}} = \psi_{i(L)}, \tag{2.16}$$

$$\begin{bmatrix} -\frac{\mu}{2} + \frac{\sigma_t h}{2} & \frac{\mu}{2} \\ -\frac{\mu}{2} & -\frac{\mu}{2} + \frac{\sigma_t h}{2} \end{bmatrix} \begin{bmatrix} \psi_L \\ \psi_R \end{bmatrix} = \begin{bmatrix} \frac{\sigma_s h}{4}\phi_L + \frac{hQ}{4} \\ \frac{\sigma_s h}{4}\phi_R + \frac{hQ}{4} - \mu\psi_{i+\frac{1}{2}} \end{bmatrix}. \tag{2.17}$$

This system is then solved on each cell across the domain by sweeping from the exterior boundary (where there is an incident angular flux) towards the interior boundary for all of the negative discrete angular cosines, followed by sweeping from the interior boundary (where there is a reflective condition) back to the exterior boundary for all positive angular cosines. The resulting angular fluxes are used to compute the scalar flux on the cell edges using the Gauss quadrature in equation (2.8).

2.2.3 Cell Centered DSA

For the diffusion step, the traditional cell-center diffusion scheme of the residual, as defined in equation (2.1), is discretized on a sub-mesh of cells with a width of $h/2$. After discretization, equation (2.1) is solved by inverting a tri-diagonal matrix, making this step computationally cheap to perform compared to the transport sweeps. However, our approach uses cell widths half the size of the transport cells, and is thus placing the diffusion cell-centers at the $1/4$ and $3/4$ marks of the transport cell:

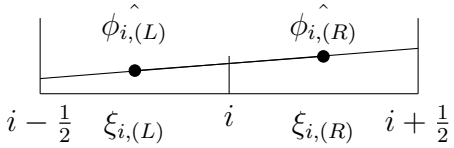

The interior fluxes are computed by interpolating from the transport edge fluxes:

$$\hat{\phi_L} = \frac{1}{4}\phi_R + \frac{3}{4}\phi_L, \tag{2.18}$$

$$\hat{\phi_R} = \frac{1}{4}\phi_L + \frac{3}{4}\phi_R. \tag{2.19}$$

Then, the following discrete version of (2.1) is solved across the domain with alternating (L) and (R) indices:

$$\frac{2}{3\sigma_t h}(\hat{\xi}_{i(L)} - \hat{\xi}_{i-1(R)}) - \frac{2}{3\sigma_t h}(\hat{\xi}_{i(R)} - \hat{\xi}_{i(L)}) + \frac{\sigma_a h}{2}\hat{\xi}_{i(L)} = \frac{\sigma_s h}{2}[\hat{\phi_L} - \hat{\phi_R}], \tag{2.20}$$

$$\frac{2}{3\sigma_t h}(\hat{\xi}_{i(R)} - \hat{\xi}_{i(L)}) - \frac{2}{3\sigma_t h}(\hat{\xi}_{i+1(L)} - \hat{\xi}_{i(R)}) + \frac{\sigma_a h}{2}\hat{\xi}_{i(R)} = \frac{\sigma_s h}{2}[\hat{\phi_R} - \hat{\phi_L}]. \tag{2.21}$$

This system can be used to construct the typical tri-diagonal matrix used in traditional diffusion, with the only difference being the source term used, which is then computed across the domain to yield the desired error terms. The resulting errors must then be extrapolated back out to the cell edges to be used as correction terms to the transport fluxes. Here we use the same linear mapping as before, only inverted:

$$\xi_L = -\frac{1}{2}\hat{\xi}_R + \frac{3}{2}\hat{\xi}_L, \tag{2.22}$$

$$\xi_R = -\frac{1}{2}\hat{\xi}_L + \frac{3}{2}\hat{\xi}_R, \tag{2.23}$$

$$\phi_L^{l+1} = \phi_L^{l+\frac{1}{2}} + \xi_L, \tag{2.24}$$

$$\phi_R^{l+1} = \phi_R^{l+\frac{1}{2}} + \xi_R. \tag{2.25}$$

Which completes the full iteration of our DSA method. With some initial guess and appropriate boundary conditions, the transport sweep can be performed, resulting in the uncorrected, half-step fluxes. These values are then interpolated to the sub-mesh cell centers. A computationally cheap, modified diffusion solver is then used to solve for the correction terms on the sub-mesh, which are extrapolated back to the transport mesh to be applied to the previous iterates flux values. With the

zero source version of the problem, we converge the spectral radius rather than the solution itself to quantitatively describe the scheme's performance. The results are further discussed in section 4 of this thesis.

3. FOURIER ANALYSIS

3.1 Description of Stability Analysis using the Fourier Ansatz

To further quantitatively describe the performance of the scheme derived in section 3, we consider the infinite homogeneous medium problem and approximate the error as exponential modes by the Fourier ansatz, yielding the following iterative system:

$$\delta\phi^{l+1} = M\delta\phi^{l} \tag{3.1}$$

where the $\delta\phi$'s represent the error in the scalar flux and M is the error reduction matrix, whose eigenvalues govern the stability of the system.

For our proposed DSA method, two separate analyses were done, one for the S_N sweep, and then another for the diffusion preconditioning step, resulting in the M described in equation (3.1). The determinent of this matrix can then be analyzed for each value of λ in the Fourier exponential mode proposed. The rate of convergence is then determined by the maximum eigenvalue over all λ's, which is our desired spectral radius.

3.1.1 Error Reduction Matrix from the Fourier Ansatz Applied to the Transport Sweeps

We start by deriving the residual form of the transport equation for our defined problem. From equation (2.5), this yields the following:

$$\mu\frac{\partial\delta\psi^{l+\frac{1}{2}}}{\partial x} + \sigma_t\delta\psi^{l+\frac{1}{2}} = \frac{\sigma_s}{2}\delta\phi^{l}. \tag{3.2}$$

Then we apply the same spacial and angular discretization scheme as before, only now our variable of interest is the error in the angular flux, not the angular flux itself. This leads to the following angle dependent equations, similar to the original transport sweep derived in equations (2.9 - 2.12):

$$\mu > 0 : \mu[\delta\psi_i^{l+\frac{1}{2}} - \delta\psi_{i-\frac{1}{2}}^{l+\frac{1}{2}}] + \frac{\sigma_t h}{2}\delta\psi_{i(L)}^{l+\frac{1}{2}} = \frac{\sigma_s h}{4}\delta\phi_{i(L)}^{l}, \tag{3.3}$$

$$\mu > 0 : \mu[\delta\psi_{i+\frac{1}{2}}^{l+\frac{1}{2}} - \delta\psi_i^{l+\frac{1}{2}}] + \frac{\sigma_t h}{2}\delta\psi_{i(R)}^{l+\frac{1}{2}} = \frac{\sigma_s h}{4}\delta\phi_{i(R)}^{l}, \tag{3.4}$$

$$\mu < 0 : \mu[\delta\psi_i^{l+\frac{1}{2}} - \delta\psi_{i-\frac{1}{2}}^{l+\frac{1}{2}}] + \frac{\sigma_t h}{2}\delta\psi_{i(L)}^{l+\frac{1}{2}} = \frac{\sigma_s h}{4}\delta\phi_{i(L)}^{l}, \tag{3.5}$$

$$\mu < 0 : \mu[\delta\psi_{i+\frac{1}{2}}^{l+\frac{1}{2}} - \delta\psi_i^{l+\frac{1}{2}}] + \frac{\sigma_t h}{2}\delta\psi_{i(R)}^{l+\frac{1}{2}} = \frac{\sigma_s h}{4}\delta\phi_{i(R)}^{l}. \tag{3.6}$$

This system is repeated for each μ in the original Gauss-Legendre quadrature used in the transport sweep. Since the angles in the Gauss-Legendre quadrature are symetric about $\mu = 0$, an absolute value of mu is used and the system is redefined to solve for ψ_+ and ψ_- , representing the directional angular flux for each absolute value angular cosine at each location on the infinite slab, yielding the following system:

$$\mu[\delta\psi_{+,i}^{l+\frac{1}{2}} - \delta\psi_{+,i-\frac{1}{2}}^{l+\frac{1}{2}}] + \frac{\sigma_t h}{2}\delta\psi_{+,i(L)}^{l+\frac{1}{2}} = \frac{\sigma_s h}{4}\delta\phi_{i(L)}^{l}, \tag{3.7}$$

$$\mu[\delta\psi_{+,i+\frac{1}{2}}^{l+\frac{1}{2}} - \delta\psi_{+,i}^{l+\frac{1}{2}}] + \frac{\sigma_t h}{2}\delta\psi_{+,i(R)}^{l+\frac{1}{2}} = \frac{\sigma_s h}{4}\delta\phi_{i(R)}^{l}, \tag{3.8}$$

$$\mu[\delta\psi_{-,i-\frac{1}{2}}^{l+\frac{1}{2}} - \delta\psi_{-,i}^{l+\frac{1}{2}}] + \frac{\sigma_t h}{2}\delta\psi_{-,i(L)}^{l+\frac{1}{2}} = \frac{\sigma_s h}{4}\delta\phi_{i(L)}^{l}, \tag{3.9}$$

$$\mu[\delta\psi_{-,i}^{l+\frac{1}{2}} - \delta\psi_{-,i+\frac{1}{2}}^{l+\frac{1}{2}}] + \frac{\sigma_t h}{2}\delta\psi_{-,i(R)}^{l+\frac{1}{2}} = \frac{\sigma_s h}{4}\delta\phi_{i(R)}^{l}. \tag{3.10}$$

We then apply the same averaging and upwinding that was used in the transport sweep discretization. This gives us the system of equations that we wish to apply the Fourier ansatz to for our analysis:

$$\mu[\frac{1}{2}[\delta\psi_{+,i(L)}^{l+\frac{1}{2}}+\delta\psi_{+,i(R)}^{l+\frac{1}{2}}]-\delta\psi_{+,i-1(R)}^{l+\frac{1}{2}}]+\frac{\sigma_t h}{2}\delta\psi_{+,i(L)}^{l+\frac{1}{2}}=\frac{\sigma_s h}{4}\delta\phi_{i(L)}^{l}, \tag{3.11}$$

$$\mu[\delta\psi_{+,i(R)}^{l+\frac{1}{2}}-\frac{1}{2}[\delta\psi_{+,i(L)}^{l+\frac{1}{2}}+\delta\psi_{+,i(R)}^{l+\frac{1}{2}}]]+\frac{\sigma_t h}{2}\delta\psi_{+,i(R)}^{l+\frac{1}{2}}=\frac{\sigma_s h}{4}\delta\phi_{i(R)}^{l}, \tag{3.12}$$

$$\mu[\delta\psi_{-,i(L)}^{l+\frac{1}{2}}-\frac{1}{2}[\delta\psi_{-,i(L)}^{l+\frac{1}{2}}+\delta\psi_{-,i(R)}^{l+\frac{1}{2}}]]+\frac{\sigma_t h}{2}\delta\psi_{-,i(L)}^{l+\frac{1}{2}}=\frac{\sigma_s h}{4}\delta\phi_{i(L)}^{l}, \tag{3.13}$$

$$\mu[\frac{1}{2}[\delta\psi_{-,i(L)}^{l+\frac{1}{2}}+\delta\psi_{-,i(R)}^{l+\frac{1}{2}}]-\delta\psi_{-,i+1(L)}^{l+\frac{1}{2}}]+\frac{\sigma_t h}{2}\delta\psi_{-,i(R)}^{l+\frac{1}{2}}=\frac{\sigma_s h}{4}\delta\phi_{i(R)}^{l}. \tag{3.14}$$

For our ansatz, we assume a single Fourier mode for each error term in our system, both in angular flux as well as in scalar flux. This gives us the following six modes that repeat across the infinite medium:

$$\delta\psi_{i(L)}\approx e^{i\lambda x_{i-\frac{1}{2}}}\delta\psi_L, \tag{3.15}$$

$$\delta\psi_{i(R)}\approx e^{i\lambda x_{i+\frac{1}{2}}}\delta\psi_R, \tag{3.16}$$

$$\delta\psi_{i+1(L)}\approx e^{i\lambda x_{i+\frac{1}{2}}}\delta\psi_L, \tag{3.17}$$

$$\delta\psi_{i-1(R)}\approx e^{i\lambda x_{i-\frac{1}{2}}}\delta\psi_R, \tag{3.18}$$

$$\delta\phi_{i(L)}\approx e^{i\lambda x_{i-\frac{1}{2}}}\delta\phi_L, \tag{3.19}$$

$$\delta\phi_{i(R)}\approx e^{i\lambda x_{i+\frac{1}{2}}}\delta\phi_R. \tag{3.20}$$

Each of which, are substituted into equations (3.11 - 3.14) to yield the following:

$$\mu[\frac{1}{2}[e^{i\lambda x_{i-\frac{1}{2}}}\delta\psi^{l+\frac{1}{2}}_{+,i(L)} + e^{i\lambda x_{i+\frac{1}{2}}}\delta\psi^{l+\frac{1}{2}}_{+,i(R)}] - e^{i\lambda x_{i-\frac{1}{2}}}\delta\psi^{l+\frac{1}{2}}_{+,(R)}] + \frac{\sigma_t h}{2}e^{i\lambda x_{i-\frac{1}{2}}}\delta\psi^{l+\frac{1}{2}}_{+,i(L)} = \frac{\sigma_s h}{4}e^{i\lambda x_{i-\frac{1}{2}}}\delta\phi^{l}_{i(L)}, \tag{3.21}$$

$$\mu[e^{i\lambda x_{i+\frac{1}{2}}}\delta\psi^{l+\frac{1}{2}}_{+,i(R)} - \frac{1}{2}[e^{i\lambda x_{i-\frac{1}{2}}}\delta\psi^{l+\frac{1}{2}}_{+,i(L)} + e^{i\lambda x_{i+\frac{1}{2}}}\delta\psi^{l+\frac{1}{2}}_{+,i(R)}]] + \frac{\sigma_t h}{2}e^{i\lambda x_{i+\frac{1}{2}}}\delta\psi^{l+\frac{1}{2}}_{+,i(R)} = \frac{\sigma_s h}{4}e^{i\lambda x_{i+\frac{1}{2}}}\delta\phi^{l}_{i(R)}, \tag{3.22}$$

$$\mu[e^{i\lambda x_{i-\frac{1}{2}}}\delta\psi^{l+\frac{1}{2}}_{-,i(L)} - \frac{1}{2}[e^{i\lambda x_{i-\frac{1}{2}}}\delta\psi^{l+\frac{1}{2}}_{-,i(L)} + e^{i\lambda x_{i+\frac{1}{2}}}\delta\psi^{l+\frac{1}{2}}_{-,i(R)}]] + \frac{\sigma_t h}{2}e^{i\lambda x_{i-\frac{1}{2}}}\delta\psi^{l+\frac{1}{2}}_{-,i(L)} = \frac{\sigma_s h}{4}e^{i\lambda x_{i-\frac{1}{2}}}\delta\phi^{l}_{i(L)}, \tag{3.23}$$

$$\mu[\frac{1}{2}[e^{i\lambda x_{i-\frac{1}{2}}}\delta\psi^{l+\frac{1}{2}}_{-,i(L)} + e^{i\lambda x_{i+\frac{1}{2}}}\delta\psi^{l+\frac{1}{2}}_{-,i(R)}] - e^{i\lambda x_{i+\frac{1}{2}}}\delta\psi^{l+\frac{1}{2}}_{-,i(L)}] + \frac{\sigma_t h}{2}e^{i\lambda x_{i+\frac{1}{2}}}\delta\psi^{l+\frac{1}{2}}_{-,i(R)} = \frac{\sigma_s h}{4}e^{i\lambda x_{i+\frac{1}{2}}}\delta\phi^{l}_{i(R)}. \tag{3.24}$$

Our equations are currently formulated in terms of $x_{i+/-\frac{1}{2}}$. It is beneficial to modify these equations to be in terms of the cell width, λh, since the medium is homogeneous and has the same cell width throughout. To achieve this, the entire system is divided by $e^{i\lambda x_i}$:

$$\mu[\frac{1}{2}[e^{-i\lambda\frac{h}{2}}\delta\psi^{l+\frac{1}{2}}_{+,i(L)} + e^{i\lambda\frac{h}{2}}\delta\psi^{l+\frac{1}{2}}_{+,i(R)}] - e^{-i\lambda\frac{h}{2}}\delta\psi^{l+\frac{1}{2}}_{+,(R)}] + \frac{\sigma_t h}{2}e^{-i\lambda\frac{h}{2}}\delta\psi^{l+\frac{1}{2}}_{+,i(L)} = \frac{\sigma_s h}{4}e^{-i\lambda\frac{h}{2}}\delta\phi^{l}_{i(L)}, \tag{3.25}$$

$$\mu[e^{i\lambda\frac{h}{2}}\delta\psi^{l+\frac{1}{2}}_{+,i(R)} - \frac{1}{2}[e^{-i\lambda\frac{h}{2}}\delta\psi^{l+\frac{1}{2}}_{+,i(L)} + e^{i\lambda\frac{h}{2}}\delta\psi^{l+\frac{1}{2}}_{+,i(R)}]] + \frac{\sigma_t h}{2}e^{i\lambda\frac{h}{2}}\delta\psi^{l+\frac{1}{2}}_{+,i(R)} = \frac{\sigma_s h}{4}e^{i\lambda\frac{h}{2}}\delta\phi^{l}_{i(R)}, \tag{3.26}$$

$$\mu[e^{-i\lambda\frac{h}{2}}\delta\psi^{l+\frac{1}{2}}_{-,i(L)} - \frac{1}{2}[e^{-i\lambda\frac{h}{2}}\delta\psi^{l+\frac{1}{2}}_{-,i(L)} + e^{i\lambda\frac{h}{2}}\delta\psi^{l+\frac{1}{2}}_{-,i(R)}]] + \frac{\sigma_t h}{2}e^{-i\lambda\frac{h}{2}}\delta\psi^{l+\frac{1}{2}}_{-,i(L)} = \frac{\sigma_s h}{4}e^{-i\lambda\frac{h}{2}}\delta\phi^{l}_{i(L)}, \tag{3.27}$$

$$\mu[\frac{1}{2}[e^{-i\lambda\frac{h}{2}}\delta\psi^{l+\frac{1}{2}}_{-,i(L)} + e^{i\lambda\frac{h}{2}}\delta\psi^{l+\frac{1}{2}}_{-,i(R)}] - e^{i\lambda\frac{h}{2}}\delta\psi^{l+\frac{1}{2}}_{-,i(L)}] + \frac{\sigma_t h}{2}e^{i\lambda\frac{h}{2}}\delta\psi^{l+\frac{1}{2}}_{-,i(R)} = \frac{\sigma_s h}{4}e^{i\lambda\frac{h}{2}}\delta\phi^{l}_{i(R)}. \tag{3.28}$$

It is trivial then to rewrite our system into a matrix equation with repeating elements for each n'th absolute value of μ in the following form:

$$A\delta\psi^{l+\frac{1}{2}} = B\delta\phi^{l}, \tag{3.29}$$

where A is a 4nx4n matrix with zeros everywhere except for along the main diagonal, which has

the form of the following 4x4 matrix repeating for each n'th absolute value of μ:

$$\begin{bmatrix} (\frac{\mu}{2}+\frac{\sigma_t h}{2})e^{-i\lambda\frac{h}{2}} & 0 & \mu(\frac{1}{2}e^{i\lambda\frac{h}{2}}-e^{-i\lambda\frac{h}{2}}) & 0 \\ -\frac{\mu}{2}e^{-i\lambda\frac{h}{2}} & 0 & (\frac{\mu}{2}+\frac{\sigma_t h}{2})e^{i\lambda\frac{h}{2}} & 0 \\ 0 & (\frac{\mu}{2}+\frac{\sigma_t h}{2})e^{-i\lambda\frac{h}{2}} & 0 & -\frac{\mu}{2}e^{i\lambda\frac{h}{2}} \\ 0 & \mu(\frac{1}{2}e^{-i\lambda\frac{h}{2}}-e^{i\lambda\frac{h}{2}}) & 0 & (\frac{\mu}{2}+\frac{\sigma_t h}{2})e^{i\lambda\frac{h}{2}} \end{bmatrix}, \tag{3.30}$$

$\delta\psi^{l+\frac{1}{2}}$ is a 4nx1 vector constisting of repeating vectors of the angular flux error for each n'th absolute value of μ:

$$\begin{bmatrix} \delta\psi^{l+\frac{1}{2}}_{+,i(L)} \\ \delta\psi^{l+\frac{1}{2}}_{-,i(L)} \\ \delta\psi^{l+\frac{1}{2}}_{+,i(R)} \\ \delta\psi^{l+\frac{1}{2}}_{-,i(R)} \end{bmatrix}, \tag{3.31}$$

B is a 4nx2 matrix that consists of the following 4x2 matrix repeating for each n'th absolute value of μ:

$$\begin{bmatrix} \frac{\sigma_s h}{4}e^{-i\lambda\frac{h}{2}} & 0 \\ 0 & \frac{\sigma_s h}{4}e^{i\lambda\frac{h}{2}} \\ \frac{\sigma_s h}{4}e^{-i\lambda\frac{h}{2}} & 0 \\ 0 & \frac{\sigma_s h}{4}e^{i\lambda\frac{h}{2}} \end{bmatrix}, \tag{3.32}$$

and $\delta\phi^l$ is a 2x1 vector of the scalar flux error:

$$\begin{bmatrix} \delta\phi^l_L \\ \delta\phi^l_R \end{bmatrix}. \tag{3.33}$$

Which means that the error in the angular flux can be solved for by a simple matrix inversion of the matrix A, giving us a similar form as equation (3.1) over the transport half-step:

$$\delta\psi^{l+\frac{1}{2}} = A^{-1}B\delta\phi^l. \tag{3.34}$$

However, in order to get the left hand side in terms of the error in the scalar flux, we must apply the same quadrature weights from the Gauss-Legendre expansion used in equation (2.4). This is accomplished by defining a new weight matrix that approximates the integral of the angular flux over the angular cosines:

$$\delta\phi^{l+\frac{1}{2}} = W\delta\psi^{l+\frac{1}{2}} = WA^{-1}B\delta\phi^{l}. \tag{3.35}$$

Here, W is a 2x4n matrix that consists of a repeating 2x4 matrix of the weights associated with each n'th absolute value of μ:

$$\begin{bmatrix} w(\mu) & w(\mu) & 0 & 0 \\ 0 & 0 & w(\mu) & w(\mu) \end{bmatrix}. \tag{3.36}$$

And thus, we have our desired error reduction matrix for our transport sweep using our Fourier ansatz:

$$C = WA^{-1}B. \tag{3.37}$$

From here on out, this error reduction matrix will be referenced as C.

3.1.2 Modified Error Reduction Matrix from the Fourier Ansatz Applied to the Two-Point Diffusion Half-Step

Next, we derive the error reduction matrix for the full DSA iteration. This is done in a similar fashion as we did for the sweep, starting with the residual of equation (2.1) (this is the residual of the residual of the diffusion equation):

$$-\frac{\partial}{\partial x}D\frac{\partial\delta\xi}{\partial x} + \sigma_a\delta\xi = \sigma_s(\delta\phi^{l} - \delta\phi^{l+\frac{1}{2}}). \tag{3.38}$$

Using the same extrapolation correction and half cell sub-mesh discretization used in deriving

the original DSA equations, the following half cell equations are derived:

$$\frac{2}{3\sigma_t h}(\delta\hat{\xi}_{i(L)} - \delta\hat{\xi}_{i-1(R)}) - \frac{2}{3\sigma_t h}(\delta\hat{\xi}_{i(R)} - \delta\hat{\xi}_{i(L)}) + \frac{\sigma_a h}{2}\delta\hat{\xi}_{i(L)} = \frac{\sigma_s h}{2}[(\frac{1}{4}\delta\phi^l_{i(R)} + \frac{3}{4}\delta\phi^l_{i(L)}) - (\frac{1}{4}\delta\phi^{l+\frac{1}{2}}_{i(R)} + \frac{3}{4}\delta\phi^{l+\frac{1}{2}}_{i(L)})], \tag{3.39}$$

$$\frac{2}{3\sigma_t h}(\delta\hat{\xi}_{i(R)} - \delta\hat{\xi}_{i(L)}) - \frac{2}{3\sigma_t h}(\delta\hat{\xi}_{i+1(L)} - \delta\hat{\xi}_{i(R)}) + \frac{\sigma_a h}{2}\delta\hat{\xi}_{i(R)} = \frac{\sigma_s h}{2}[(\frac{3}{4}\delta\phi^l_{i(R)} + \frac{1}{4}\delta\phi^l_{i(L)}) - (\frac{3}{4}\delta\phi^{l+\frac{1}{2}}_{i(R)} + \frac{1}{4}\delta\phi^{l+\frac{1}{2}}_{i(L)})]. \tag{3.40}$$

Here, for each full transport cell, equation (3.39) is the left hand half cell equation and (3.40) is the right hand half cell equation.

Next, we apply a similar fourier ansatz as before, assuming a single mode at each point for each error term:

$$\delta\phi_{i(L)} \approx e^{i\lambda x_{i-\frac{1}{2}}}\delta\phi_L, \tag{3.41}$$

$$\delta\phi_{i(R)} \approx e^{i\lambda x_{i+\frac{1}{2}}}\delta\phi_R, \tag{3.42}$$

$$\delta\hat{\xi}_{i(L)} \approx e^{i\lambda x_{i-\frac{1}{4}}}\delta\hat{\xi}_L, \tag{3.43}$$

$$\delta\hat{\xi}_{i(R)} \approx e^{i\lambda x_{i+\frac{1}{4}}}\delta\hat{\xi}_R, \tag{3.44}$$

$$\delta\hat{\xi}_{i+1(L)} \approx e^{i\lambda x_{i+\frac{3}{4}}}\delta\hat{\xi}_L, \tag{3.45}$$

$$\delta\hat{\xi}_{i-1(R)} \approx e^{i\lambda x_{i-\frac{3}{4}}}\delta\hat{\xi}_R. \tag{3.46}$$

Plugging these approximations into equations (3.39) and (3.40), we get the following:

$$-\frac{2}{3\sigma_t h}(e^{i\lambda x_{i+\frac{1}{4}}}\delta\hat{\xi}_R - 2e^{i\lambda x_{i-\frac{1}{4}}}\delta\hat{\xi}_L + e^{i\lambda x_{i-\frac{3}{4}}}\delta\hat{\xi}_R) + \frac{\sigma_a h}{2}e^{i\lambda x_{i-\frac{1}{4}}}\delta\hat{\xi}_L = \frac{\sigma_s h}{2}[\frac{1}{4}e^{i\lambda x_{i+\frac{1}{2}}}(\delta\phi^l_R - \delta\phi^{l+\frac{1}{2}}_R) + \frac{3}{4}e^{i\lambda x_{i-\frac{1}{2}}}(\delta\phi^l_L - \delta\phi^{l+\frac{1}{2}}_L)], \tag{3.47}$$

$$-\frac{2}{3\sigma_t h}(e^{i\lambda x_{i+\frac{3}{4}}}\delta\hat{\xi}_L - 2e^{i\lambda x_{i+\frac{1}{4}}}\delta\hat{\xi}_R + e^{i\lambda x_{i-\frac{1}{4}}}\delta\hat{\xi}_L) + \frac{\sigma_a h}{2}e^{i\lambda x_{i+\frac{1}{4}}}\delta\hat{\xi}_R = \frac{\sigma_s h}{2}[\frac{3}{4}e^{i\lambda x_{i+\frac{1}{2}}}(\delta\phi^l_R - \delta\phi^{l+\frac{1}{2}}_R) + \frac{1}{4}e^{i\lambda x_{i-\frac{1}{2}}}(\delta\phi^l_L - \delta\phi^{l+\frac{1}{2}}_L)]. \tag{3.48}$$

Again, our equations are currently formulated in terms of $x_{i+/-\frac{1}{2}}$. Like before, it is beneficial to modify these equations to be in terms of the cell width, λh, so we again divide the entire system by $e^{i\lambda x_i}$:

$$-\frac{2}{3\sigma_t h}(e^{i\lambda\frac{h}{4}}\delta\hat{\xi}_R - 2e^{-i\lambda\frac{h}{4}}\delta\hat{\xi}_L + e^{-i\lambda\frac{3h}{4}}\delta\hat{\xi}_R) + \frac{\sigma_a h}{2}e^{-i\lambda\frac{h}{4}}\delta\hat{\xi}_L = \frac{\sigma_s h}{2}[\frac{1}{4}e^{i\lambda\frac{h}{2}}(\delta\phi_R^l - \delta\phi_R^{l+\frac{1}{2}}) + \frac{3}{4}e^{-i\lambda\frac{h}{2}}(\delta\phi_L^l - \delta\phi_L^{l+\frac{1}{2}})], \tag{3.49}$$

$$-\frac{2}{3\sigma_t h}(e^{i\lambda\frac{3h}{4}}\delta\hat{\xi}_L - 2e^{i\lambda\frac{h}{4}}\delta\hat{\xi}_R + e^{-i\lambda\frac{h}{4}}\delta\hat{\xi}_L) + \frac{\sigma_a h}{2}e^{i\lambda\frac{h}{4}}\delta\hat{\xi}_R = \frac{\sigma_s h}{2}[\frac{3}{4}e^{i\lambda\frac{h}{2}}(\delta\phi_R^l - \delta\phi_R^{l+\frac{1}{2}}) + \frac{1}{4}e^{-i\lambda\frac{h}{2}}(\delta\phi_L^l - \delta\phi_L^{l+\frac{1}{2}})]. \tag{3.50}$$

It is trivial now to see that this is also a matrix equation of the following form:

$$D\delta\hat{\xi} = E(\delta\phi^l - \delta\phi^{l+\frac{1}{2}}), \tag{3.51}$$

where D is the following 2x2 matrix:

$$\begin{bmatrix} (\frac{4}{3\sigma_t h} + \frac{\sigma_a h}{2})e^{-i\lambda\frac{h}{4}} & -\frac{2}{3\sigma_t h}(e^{i\lambda\frac{h}{4}} + e^{-i\lambda\frac{3h}{4}}) \\ -\frac{2}{3\sigma_t h}(e^{i\lambda\frac{3h}{4}} + e^{-i\lambda\frac{h}{4}}) & (\frac{4}{3\sigma_t h} + \frac{\sigma_a h}{2})e^{i\lambda\frac{h}{4}} \end{bmatrix}, \tag{3.52}$$

$\delta\hat{\xi}$ is the following 2x1 vector of the error of the error on the left and right fluxes on each cell:

$$\begin{bmatrix} \delta\hat{\xi}_L \\ \delta\hat{\xi}_R \end{bmatrix}, \tag{3.53}$$

E is the following 2x2 matrix:

$$\begin{bmatrix} \frac{3\sigma_s h}{8}e^{-i\lambda\frac{h}{2}} & \frac{\sigma_s h}{8}e^{i\lambda\frac{h}{2}} \\ \frac{\sigma_s h}{8}e^{-i\lambda\frac{h}{2}} & \frac{3\sigma_s h}{8}e^{i\lambda\frac{h}{2}} \end{bmatrix}, \tag{3.54}$$

$\delta\phi^l$ is the following 2x1 vector of the scalar flux error before the sweep:

$$\begin{bmatrix} \delta\phi_L^l \\ \delta\phi_R^l \end{bmatrix}, \tag{3.55}$$

and $\delta\phi^{l+\frac{1}{2}}$ is the following 2x1 vector of the scalar flux error after the sweep:

$$\begin{bmatrix} \delta\phi_L^{l+\frac{1}{2}} \\ \delta\phi_R^{l+\frac{1}{2}} \end{bmatrix}. \tag{3.56}$$

We wish to derive the error reduction matrix in the form of equation (3.1), so we then invert D to arrive at the following form:

$$\delta\hat{\xi} = D^{-1}E(\delta\phi^l - \delta\phi^{l+\frac{1}{2}}). \tag{3.57}$$

We then also recognize that $\phi^{l+\frac{1}{2}}$ can be rewritten in terms of C by equations (3.35) and (3.37):

$$\delta\hat{\xi} = D^{-1}E(\delta\phi^l - C\delta\phi^l). \tag{3.58}$$

However, equation (3.58) only applies to the error of the error at the DSA points on the sub-mesh. In order to get the correct error reduction matrix for the full DSA iteration, we need to redefine this in terms of the error in the correction term at the transport cell edges, represented as a $\delta\xi$. This is accomplished by mapping back using our linear extrapolation:

$$\delta\xi_{i(L)} = \frac{3}{2}\delta\hat{\xi}_{i(L)} - \frac{1}{2}\delta\hat{\xi}_{i(R)}, \tag{3.59}$$

$$\delta\xi_{i(R)} = \frac{3}{2}\delta\hat{\xi}_{i(R)} - \frac{1}{2}\delta\hat{\xi}_{i(L)}. \tag{3.60}$$

Which must also have the same Fourier ansatz applied to it, yielding:

$$\delta\xi_L = \frac{3}{2}e^{i\lambda\frac{h}{4}}\delta\hat{\xi}_L - \frac{1}{2}e^{i\lambda\frac{3h}{4}}\delta\hat{\xi}_R, \tag{3.61}$$

$$\delta\xi_R = \frac{3}{2}e^{-i\lambda\frac{h}{4}}\delta\hat{\xi}_R - \frac{1}{2}e^{-i\lambda\frac{3h}{4}}\delta\hat{\xi}_L. \tag{3.62}$$

We then rewrite this as the following matrix equation:

$$\delta\xi = F\delta\hat{\xi}, \tag{3.63}$$

where $\delta\xi$ is the vector of the extrapolated errors of the errors:

$$\begin{bmatrix} \delta\xi_L \\ \delta\xi_R \end{bmatrix}, \tag{3.64}$$

and F is the matrix for the mapping from the sub mesh to the original mesh for the sweep:

$$\begin{bmatrix} \frac{3}{2}e^{i\lambda\frac{h}{4}} & -\frac{1}{2}e^{i\lambda\frac{3h}{4}} \\ -\frac{1}{2}e^{-i\lambda\frac{3h}{4}} & \frac{3}{2}e^{-i\lambda\frac{h}{4}}. \end{bmatrix} \tag{3.65}$$

If we substitute this mapping into equation (3.58) for $\delta\hat{\xi}$, $\delta\xi$ can be represented in the following way:

$$\delta\xi = FD^{-1}E(\delta\phi^l - C\delta\phi^l). \tag{3.66}$$

Which can then be used to solve for the error reduction matrix of the total error at the end of each DSA iteration, defined as:

$$\delta\phi^{l+1} = \delta\phi^{l+\frac{1}{2}} - \delta\xi. \tag{3.67}$$

By plugging in equations (3.35), (3.37), and (3.66) into equation 92, we can get the following matrix equation:

$$\delta\phi^{l+1} = C\delta\phi^l - FD^{-1}E(\delta\phi^l - C\delta\phi^l). \tag{3.68}$$

This can be rewritten in the form of equation (3.1), the desired form of the error reduction matrix over the full DSA iteration that we wish to analyze, yielding:

$$\delta\phi^{l+1} = [C - F(D^{-1}(E - EC))]\delta\phi^l. \tag{3.69}$$

Which we further simplify to the following 2x2 error reduction matrix, M, whose eigenvalues quantitatively describe the stability of the system:

$$M = C - F(D^{-1}(E - EC)). \tag{3.70}$$

The largest eigenvalues of matrix M for each λ, converge to the spectral radius of our proposed two-point DSA numerical method. Thus, we can iterate over the repeating domanin of λ from 0 to $\frac{2\pi}{h}$ for each tested configuration and have a quantitative description of whether or not the method is stable under those tested conditions. The results of these tests are included in section, and compared to the computational experiments using the method derived in section 2.

4. COMPUTATIONAL RESULTS

4.1 Description of Test Problems

For simplicity, the base computational test problem analyzed assumes a 1000 cm slab with a vacuum boundary condition on the right, a reflective condition on the left, a total cross-section of 1 cm^{-1}, variable absorption and scattering cross-sections, 1000 cells, and an 8 point Gauss-Legendre quadrature expansion. The zero source version of the problem was used in all tests performed. This allows for the iterative solution to be the error, eliminating issues with roundoff errors and the solution converging before the spectral radius. The slab size was varied to solve for the spectral radius for different cell sizes. The spectral radius was calculated by taking a ratio of the L2 norms of differences of successive scalar flux iterates and converging on this value with a tolerance of 1E-5:

$$\rho = (\frac{\Sigma_i^N[(\phi_i^{l+1})^2 - (\phi_i^l)^2]}{\Sigma_i^N[(\phi_i^l)^2 - (\phi_i^{l-1})^2]})^{\frac{1}{2}}, \tag{4.1}$$

which becomes the following for the zero source problem:

$$\rho = (\frac{\Sigma_i^N(\phi_i^{l+1})^2}{\Sigma_i^N(\phi_i^l)^2})^{\frac{1}{2}}. \tag{4.2}$$

These values were tabulated for varying cross-sections and cell sizes below. The results are organized by values of c, the scattering ratio, defined as:

$$c = \sigma_s/\sigma_t, \tag{4.3}$$

as well as by the cell sizes, which were varied by powers of 10, from 0.01 cm to 10 cm for each tested value of c.

We also solve for the eigenvalues of the error reduction matrix M, from equation (3.70) derived in Section 3, iterating λ over 0 to $2\frac{\pi}{h}$ for the same combination of c and h as in the computational test. The largest eigenvalues for each of these combinations of c and h were tabulated as the

spectral radii for each problem.

4.2 Comparison of Computational Test and Fourier Analysis Results

The following tables, table (4.1), tabulate the results for both the computational tests and the Fourier analysis respectively. In each of these tables, the data is organized into sets by the scattering ratio, c. Within each set, the resulting spectral radius, ρ, for each magnitude change in in cell width, h, is recorded. Both tables are provided below in the same format, adjacent to one another, so that the reader may more easily compare the results directly.

Table 4.1: Computational Test and Fourier Analysis Results

c = 1.0			c = 0.99			c = 0.95		
h(cm)	**ρ Computational**	**ρ Fourier Analysis**	**h(cm)**	**ρ Computational**	**ρ Fourier Analysis**	**h(cm)**	**ρ Computational**	**ρ Fourier Analysis**
0.01	0.222	0.222	0.01	0.219	0.219	0.01	0.206	0.206
0.1	0.229	0.229	0.1	0.226	0.226	0.1	0.213	0.213
1.0	0.572	0.575	1.0	0.565	0.567	1.0	0.534	0.537
10.0	2.825	2.829	10.0	2.034	2.037	10.0	0.934	0.935

c = 0.90			c = 0.50			c = 0.30		
h(cm)	**ρ Computational**	**ρ Fourier Analysis**	**h(cm)**	**ρ Computational**	**ρ Fourier Analysis**	**h(cm)**	**ρ Computational**	**ρ Fourier Analysis**
0.01	0.191	0.191	0.01	0.093	0.093	0.01	0.053	0.053
0.1	0.197	0.198	0.1	0.097	0.098	0.1	0.056	0.056
1.0	0.497	0.499	1.0	0.241	0.242	1.0	0.136	0.137
10.0	0.535	0.536	10.0	0.072	0.072	10.0	0.031	0.031

c = 0.10		
h(cm)	**ρ Computational**	**ρ Fourier Analysis**
0.01	0.017	0.017
0.1	0.018	0.018
1.0	0.043	0.043
10.0	0.008	0.008

4.3 Analysis of Results

Comparing these results, one can see that the computational tests and Fourier analysis results are in agreement, as expected. This reinforces that the Fourier analysis was performed correctly on the desired method that was initially analyzed by the computational tests. In these results, a spectral radius greater than 1.0 would indicate that the result was non-convergent and that the method was unstable under those conditions. In both the computational tests, as well as the Fourier analysis, the results show convergence, regardless of cell width, for the cases where the scattering ratio was

equal to 0.10, 0.30, 0.50, 0.90, and 0.95. However, in the cases dominated by scattering, where the scattering ratio equaled 0.99, and 1.0, the method was non-convergent when the cell width was equal to 10.0 cm. Regardless of scattering ratio, there is a dependence on the cell width for the spectral radius.

There is also an observable trend of slower convergence as the scattering ratio increases. While this is expected, the amount that the convergence slows for each of the 10.0 cm cases indicates poor performance in high scattering problems with optically thick cells, even when convergent. In the problems with a scattering ratio higher than 0.90, the performance can be comparable to traditional DSA only in the optically thin cases where the cell width is much smaller than the mean-free path.

5. SUMMARY, CONCLUSIONS, AND FUTURE WORK

5.1 Summarization of Work

The primary objective of this research was to analyze the effects of having two diffusion cells per transport cell in a DSA method where the transport step was discretized with a lumped linear discontinuous Galerkin approximation. This work was inspired, though not equivalent to, work recently publish by Dr. Ryosuke Park at Los Alamos National Laboratory. For our analysis, a homogeneous, 1-D slab geometry problem with isotropic scattering and a zero source term was derived and tested. We then performed a Fourier analysis on the infinite medium equivalent of the problem, determining the spectral radius from the derived reduction matrix for our the proposed method. The results from both the test problem and the Fourier analysis were tabulated for comparison and analysis. These results were organized by scattering ratio and cell width over various tests. Discussion of these results are in section (4) of this thesis.

5.2 Conclusions

The results of our analysis show that the method is conditionally unstable. For scatter dominated problems with cell widths much larger than the mean-free path, the method becomes non-convergent. Furthermore, in the pure scattering case, the method was comparable to traditional DSA only when the cell widths were much smaller than the mean-free path. Thus, this approach by itself is not a practical alternative to more traditional DSA schemes. Also, this means that the stability gained in Ryosuke's approach was not due to having two diffusion cells per transport cell by itself, and that there must be some other reason for the gained stability.

5.3 Future Work

Given these results, it would be very interesting to derive an exact linear equivalent to Ryosuke's method to analyze as well, in order to determine what allows for such an approach to be stable. As such, there could be ample future work in determining exactly how he has manage to achieve unconditional stability even when his diffusion discretization is not consistent with his transport

discretization. Our work has shown that this is not due to having multiple diffusion cells per transport cell, at least not by itself. There must be some other reason for this gained stability and there could be much to gain by further analysis.

REFERENCES

[1] W. F. Miller and E. E. Lewis, "Computational methods of neutron transport," (1993).

[2] R. E. Alcouffe, "Diffusion synthetic acceleration methods for the diamond-differenced discrete-ordinates equations," *Nuclear Science and Engineering, 64, 344-355*, (1977).

[3] Y. Wang, H. Zhang, and R. Martineau, "Diffusion acceleration schemes for the self-adjoint angular flux formulation with void treatment," *Nuclear Science and Engineering, 176, 201-225*, (2014).

[4] M. L. Adams and E. W. Larsen, "Fast iterative methods for discrete-ordinates particle transport calculations," *Progress in Nuclear Engineering, 40, 3-159*, (2002).

[5] E. W. Larsen, "Unconditionally stable diffusion-synthetic acceleration methods for the slab geometry discrete ordinates equations. part 1: Theory," *Nuclear Science and Engineering, 82, 47-63*, (1982).

[6] M. L. Adams and W. Martin, "Diffusion synthetic acceleration of discontinuous finite element transport iterations," *Nuclear Science and Engineering, 111, 145-167*, (1992).

[7] E. W. Larsen, "Diffusion-synthetic acceleration methods for the discrete-ordinates equations,"

[8] J. A. Wilbert, H. Park, and D. A. Knoll, "A comparison of acceleration methods for solving the neutron transport k-eigenvalue problem," *Journal of Computational Physics, 274, 681-694*, (2014).

[9] L. Chacon, G. Chen, D. A. Knoll, C. Newman, H. Park, W. Taitano, J. A. Wilbert, and G. Womeldorf, "Multiscale high-order/low-order (holo) algorithms and applications," *Journal of Computational Physics, 330, 21-45*, (2017).

[10] H. Park, "Towards asymptotic diffusion limit preserving high-order, low-order method," *Nuclear Science and Engineering, 194, 952-970*, (2020).